POLITECNICO DI TORINO
Repository ISTITUZIONALE

Influence of MTPA Trajectory Evaluation on Synchronous Machines Performance

Original
Influence of MTPA Trajectory Evaluation on Synchronous Machines Performance / Sala, G., Ferrari, S., Pellegrino, G., Bianchini, C., Davoli, M.. - (2025), pp. 1-6. (2025 IEEE Workshop on Electrical Machines Design, Control and Diagnosis (WEMDCD) Valletta, Malta 09-10 April 2025) [10.1109/wemdcd61816.2025.11014114].

Availability:
This version is available at: 11583/3001238 since: 2025-06-24T13:08:03Z

Publisher:
IEEE

Published
DOI:10.1109/wemdcd61816.2025.11014114

Terms of use:

This article is made available under terms and conditions as specified in the corresponding bibliographic description in the repository

Publisher copyright
IET postprint/Author's Accepted Manuscript (con refereeing)

(Article begins on next page)

18 October 2026

Influence of MTPA Trajectory Evaluation on Synchronous Machines Performance

Giada Sala
Department of Engineering "Enzo Ferrari"
University of Modena and Reggio Emilia
Modena, Italy
0000-0001-8024-5355

Simone Ferrari
Energy Department "Galileo Ferraris"
Politecnico di Torino
Torino, Italy
0000-0002-4100-1590

Gianmario Pellegrino
Energy Department "Galileo Ferraris"
Politecnico di Torino
Torino, Italy
0000-0003-4264-1917

Claudio Bianchini
Department of Engineering "Enzo Ferrari"
University of Modena and Reggio Emilia
Modena, Italy
0000-0001-5384-8177

Matteo Davoli
Raw Power S.r.l.
Via F. Zoboli, 9 - 42124
Reggio Emilia, Italy
matteo.davoli@rawpowergroup.it

***Abstract*—Interior permanent magnet machines are characterized by high efficiency over a wide speed range. The optimal performance of these motors can be achieved by implementing the appropriate control strategies: Maximum Torque per Ampere (MTPA), Flux Weakening (FW) and Maximum Torque per Volt (MTPV). The optimal MTPA control trajectories can be found with different methods employing an inductance based model or a flux based model. In principle, the two methods are the equivalent, however, the different numerical method for the evaluation of the control trajectory can lead to slightly different results. Four motors are chosen for the analysis: an IPM machine, a pure reluctance machine, a SPM machine and a reluctance assisted machine. The results obtained from the two the models are compared with 2D-FEA simulation results.**

***Index Terms*—electrical machines, motor control, MTPA, non linear magnetic model**

I. Introduction

Interior permanent magnet (IPM) machines are largely adopted in industrial, automotive [1], aerospace [2] and marine [3] applications thanks to their high efficiency over a wide speed range. The optimal performance of these motors can be reached by implementing the appropriate control strategies: Maximum Torque per Ampere (MTPA), Flux Weakening (FW) [4] and Maximum Torque per Volt (MTPV).

Thanks to flux-weakening, the torque production capabilities are extended at higher speeds by applying stator current to counteract rotor magnet flux.

A complete analytical expression of these control trajectories is reported in [5] for both linear and non linear motor model. The computed trajectories are tested experimentally and the obtained results are good.

Optimal MTPA control trajectory can be found with different methods, the most important thing is to include in the analysis a good non linear model of the machine. Authors in [6] propose an original strategy to compensate steady state MTPA tracking errors due to non linear flux maps. Indeed, actual synchronous machines present strongly non-linear behaviors, that can cause a wide variation of the machine parameters in the operating range [7]. In [8] the state of art of the work relating to MTPA techniques are classified in machine parameters independent and machine parameters dependent, according to the manner of handling the uncertainties of machine parameters in MTPA operation.

Numerical methods can be used for the implementation online of an optimal MTPA control strategy. In [9] numerical algorithms to achieve accuate MTPA control are proposed. These algorithms can operate also considering highly saturated conditions.

Authors in [10] present an analysis of different aspects of the MTPA control trajectory implementation for IPM machines, comparing two different techniques: a non linear model based MTPA profile and a technique based on the maximization of the motor input power versus stator current (MPPA). These control techniques are analyzed considering both steady state and transient conditions.

In this paper a comparison between different methods for the computation of the optimal MTPA trajectory is reported. For each method the non linear model of the machine is considered through flux and inductance maps, computed with 2D Finite Element Analysis (2D-FEA) models. The obtained trajectories are compared with the trajectory obtained via 2-D FEA. The software used for 2-D FEA simulations is FEMM [11].

The paper is organized as follows. Firstly, Section II introduces the benchmark motors that will be adopted for the comparison. In Section III the closed-form solution for MTPA control trajectory is reported when a linear motor model is considered. Then, Section IV presents the methods adopted for the MTPA control trajectory computation when a non linear motor model is considered. Finally, in Section V the presented methods are compared and validated against 2D-FEA simulations.

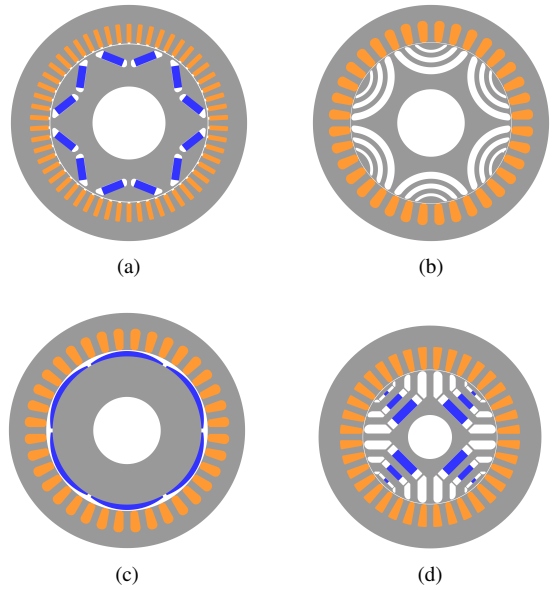

Fig. 1. Cross-sections of the four benchmark machines: a) IPM, b) SyR, c), SPM and d) PM-SyR.

II. Benchmark Motors

Four synchronous machines are considered in the following, covering several combination of magnetic anisotropy, PM strength and lamination saturation. The four motors are:

- A V-shape IPM machine (IPM);
- A pure synchronous reluctance machine (SyR) [12], [13];
- A Surface-mounted PM machine with rounded PMs (SPM) [14];
- A PM-assisted synchronous reluctance machine (PM-SyR) [15].

Their cross-sections are reported in Fig. 1, while their rating data are listed in Tab. I. Besides the geometries and nameplate data, the motors model are part of the SyR-e default library [16]. Indeed, flux and torque maps are computed with 2D-FEA simulations and will represent the baseline of the following analysis. It is worth mention that simulated models will be adopted in the following, however, the presented methods can be applied also on experimental setup, employing real machines.

TABLE I
Motor Parameters.

Parameter	*IPM*	*SyR*	*SPM*	*PM-SyR*	*Unit*
p	3	3	3	2	-
Q	54	36	36	36	-
D_e	225	175	175	170	mm
D_i	151.3	119.6	119.6	102.8	mm
g	0.7	0.325	0.325	0.325	mm
m	3	3	3	3	-
I_s	250	40	20	22	A
V_{DC}	550	565	565	310	V

III. MTPA Control Trajectory in Linear Model

When a linear model of the machine is considered, a closed-form solution for the MTPA control trajectory can be found analytically. Starting from the general IPM machine voltage equation in the rotating d-q reference frame reported in (1).

$$[v]_{dq} = R\,[i]_{dq} + \frac{d}{dt}\,[\lambda]_{dq} + jp\omega_m\,[\lambda]_{dq} \tag{1}$$

The torque can be expressed according to

$$T = \frac{3}{2}p\left[\lambda_{pm} i_q + i_d i_q\left(L_d - L_q\right)\right] \tag{2}$$

Where i_d and i_q current vectors can be expressed as a function of the current module I and the current angle γ.

$$\begin{cases} i_d &= I\cos\gamma \\ i_q &= I\sin\gamma \end{cases} \tag{3}$$

So replacing (3) in (2), torque can be expressed as follows.

$$T = \frac{3}{2}p\left[\lambda_{pm} I\sin\gamma + I^2\sin\gamma\cos\gamma\left(L_d - L_q\right)\right] \tag{4}$$

The MTPA control trajectory is defined as the locus in the i_d and i_q plane where the torque is maximum considering a fixed current amplitude. So, the analytical expression can be found computing the derivative of the ratio between the torque and the current module with respect to the curent angle γ set equal to zero, as in (5).

$$\frac{d}{d\gamma}\left(T/I\right) = 0 \tag{5}$$

$$\lambda_{pm}\cos\gamma + I\left(\sin\gamma^2 - \cos\right)\left(L_d - L_q\right) = 0 \tag{6}$$

So the current angle can be found according to

$$\gamma = \arccos\frac{\lambda_{pm}}{4I\left(L_d - L_q\right)}\left[1 \pm \sqrt{1 + 8\frac{I^2\left(L_d - L_q\right)^2}{\lambda_{pm}^2}}\right] \tag{7}$$

Nevertheless this result is obtained with the assumption of a linearized machine model where the cross coupling between each phase and the saturation effects are both neglected.

IV. MTPA Control Trajectory in Non Linear Models

To find a the correct MTPA trajectory, that account for all the non-linear motor behaviors, the complete non-linear model of the machine must be considered. The motor can be represented through inductance maps or through flux maps. Hereafter two different ways to find the optimal MTPA control trajectory are presented and, then, compared with 2D-FEA results.

Even if the MTPA can be mathematically defined as a curve, it is worth mention that, for several machines, it is possible to define an MTPA region instead of a single curve. This is especially true when different control target are considered, as loss minimization and torque ripple mitigation. Fig. 2 reports

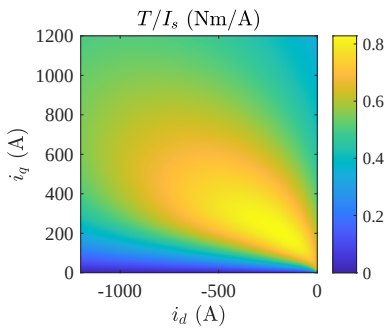

Fig. 2. Ratio of the torque and the current module of an IPM motor in the $i_d - i_q$ plane.

the torque constant contours for the IPM benchmark. This index, that is defined as the ratio between torque and peak phase current, is index of the MTPA region and it is possible to notice that the maximum values are not exactly on a well defined line.

It is interesting to notice that when the machine saturates the $\frac{T}{I_s}$ ratio reduces and the MTPA region is less evident. The maximum torque is reached when the machine saturates independently from the current angle that is used.

A. Inductance Based Method

The method considered is the same described in [17]. When inductance maps are adopted to model motor non linearities, the MTPA curve cannot be expressed in a closed form as shown in Section III. So a numeric algorithm is implemented. For each value of current module I and current angle γ an operating point in the second quadrant of the $i_d - i_q$ plane is identified and for each operating point it is possible to interpolate the inductance on d and on q axis from the maps obtained via 2D-FEA. Then for each value of I, the maximum torque is computed with Eq. 2 comparing the matrix elements corresponding to each values of γ. So the MTPA curve is found.

The inductance maps are computed through 2-D FEA simulations using frozen permeability method.

This method is easy to understand but has some limitations:

- When the torque is computed the magnet flux contribution is assumed constant in every operating point.
- An inversion of the saliency can be a problem for this method, leading to an MTPA control trajectory that can fall in the first quadrant. However, in real applications, the optimal control strategy is still in the second quadrant.

B. Flux Based Method

Another more general method to compute the MTPA, is to operate directly on flux linkage and torque maps, avoiding the computation of inductances and overcoming the issue related to PM flux linkage variation and inverse saliency. In a general framework, the magnetic model of synchronous machines can be expressed through maps as:

$$\begin{cases} \lambda_d = \mathbf{\Lambda}_d(i_d, i_q) \\ \lambda_q = \mathbf{\Lambda}_q(i_d, i_q) \end{cases} \tag{8}$$

where maps function of (i_d, i_q) are written with capital bold fonts. Torque map can be obtained from flux maps, by applying the torque quation element-wise:

$$\mathbf{T} = \frac{3}{2} p \cdot (\mathbf{\Lambda}_d \odot \mathbf{I}_q - \mathbf{\Lambda}_q \odot \mathbf{I}_d) \tag{9}$$

where the symbol $\odot$ represent the element-wise product of two matrices. It is worth noting that torque map can be directly retrieved from FEA simulations or, in case of experimental maps, it can be directly measured. The MTPA trajectory can be directly computed from torque map through iterative process, as implemented in [16]. The workflow is depicted in Fig. 3 for the IPM benchmark machine. First of all, a current amplitude vector I_{vect} is defined, from 0 to the maximum current I_{max}. The example uses current levels, however for an accurate trajectory computation, more current level can be adopted. Then, for each current I_i:

1) the current contour I_i is identified over the maps, at the coordinates $(i_{d,tmp}, i_{q,tmp})$. These correspond to portion of circles on the dq plane and are highlighted with colored lines in Fig. 3a;
2) the torque curve T_{tmp} is interpolated from torque map, as:
$$T_{tmp} = \mathbf{T}(i_{d,tmp}, i_{q,tmp}) \tag{10}$$
and represent the torque variation with the current angle γ, as reported in Fig. 3b;
3) the maximum point $T_i = \max(T_{tmp})$ over the torque curve is identified, together with the corresponding current angle γ_i. This is the MTPA point at the current I_i and it is highlighted in Fig. 3 wit colored dots.
4) the dq currents corresponding to I_i and γ_i are computed and stored in separate vectors.

The process can be applied to each kind of motor, with no limitation of anisotropy, PM strength and saturation. The workflow can be adopted also for the MTPV locus, by substituting the current vector amplitude vector I_{vect} with a flux linkage amplitude vector λ_{vect}.

V. Comparison with 2-D FEA Results

The MTPA control trajectories found with the two methods described in Section IV are compared with 2-D FEA simulations results for each motor.

A polar grid in the dq plane is defined for each motor with 10 current levels and a current angle step of 2°, around the MTPA curves identified with the previous method. For each operating point, several rotor positions are simulated, to correctly account for the harmonic and compute the average torque. Then, for each current level, the maximum torque point is identified, building the FEA-computed MTPA locus.

A. IPM

The resulting MTPA control trajectory obtained for the IPM machine is shown in Fig. 4. The trajectories computed from the two models proposed are similar and corresponds to the results obtained via 2D-FEA.

According to Fig. 5 b), the torque generated as a function of the current module is nearly the same. So the machine is working inside the MTPA operating region, which is the one highlighted in yellow in Fig. 5 a).

B. SyR

When a SyR machine is considered, the two methods proposed allow to obtain almost the same MTPA control trajectory which matches with 2D-FEA simulations results.

In this case the motor has no magnet, so there is no d-axis flux variation due to magnet operating point. Fig. 6 shows the MTPA control trajectories found for the SyR machine.

Fig. 7 a) shows the ratio of the torque and the current module of the SyR motor in the $i_d - i_q$ plane. In this case, the MTPA region is less evident since there is no magnet. Indeed, for low current levels, the magnetizing current and the absence of a PM flux linkage makes the T/I ratio quite small. Fig. 7 b) shows the torque as a function of the current module in MTPA conditions.

C. SPM

The two methods are applied also for the SPM machine. In most of traditional industrial applications, SPM machines are powered considering an MTPA current angle of 90 degrees. Nevertheless, sometimes a negative d-axis current component can be introduced to correctly track the MTPA trajectory as the iron saturation induces a small magnetic anisotropy in the motor. According to the results obtained, reported in Fig. 8, the inductance based method gives as a result a constant MTPA angle equal to 90 degrees. This result is quite different from the one obtained with the flux based method, which corresponds to the optimal MTPA control trajectory obtained via 2D-FEA.

As stated before, the MTPA is actually a region. Fig.9 a) shows the ratio between the torque and the current module in the $i_d - i_q$ plane. Here the yellow region is the MTPA region, where the torque obtained as an output is almost the same but the efficiency can change. In Fig. 5 b) the torque as a function of the current module is reported for the SPM machine. So even if the two trajectories obtained are slightly different, the output torque given a certain current module is the same.

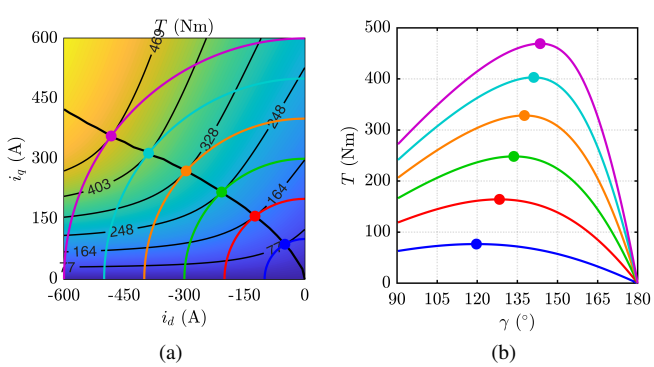

Fig. 3. Computation of MTPA from torque map. Example with 7 current level on IPM motor benchmark. (a) current and torque contours on the (i_d, i_q) plane and (b) torque curves at constant current.

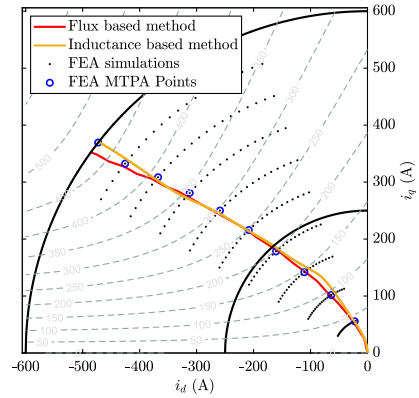

Fig. 4. MTPA control trajectories obtained for the IPM machine.

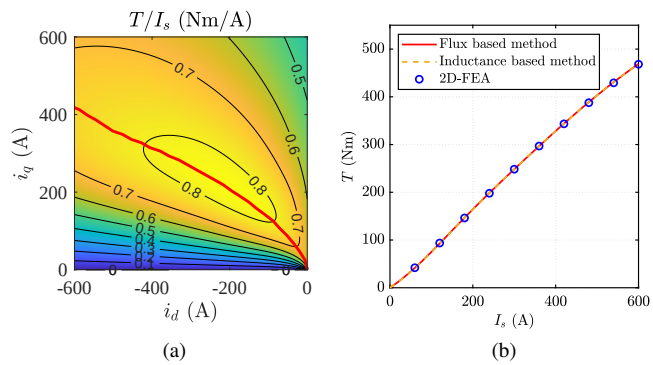

Fig. 5. a) Ratio of the torque and the current module of the IPM motor in the $i_d - i_q$ plane, b) Torque versus current module in MTPA conditions for the IPM machine.

D. PM-SyR

The MTPA control trajectories obtained for the PM-SyR machine are reported in Fig. 10. Inside the nominal current limit circle the two methods gives a similar control trajectory, which is near to the one obtained via 2D-FEA. When the current exceeds its nominal value, the two trajectories obtained from the models are different. This behavior is mainly due to the fact that the inductance based method does not consider the magnet flux variation. This method could be improved introducing a lookup table with the value of the magnet flux in every operating point.

Fig. 11 a) shows the MTPA operating region in the $i_d - i_q$ plane highlighted in yellow an Fig. 11 b) shows the torque generated from the motor following the three different MTPA control trajectories found before. The output torque is almost

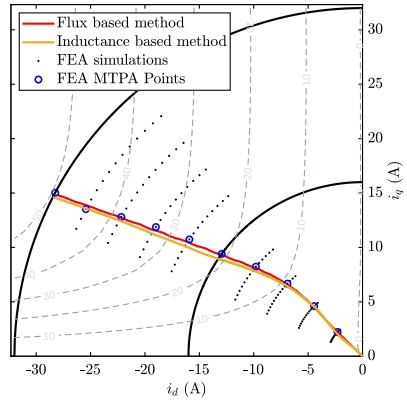

Fig. 6. MTPA control trajectories obtained for the SyR machine.

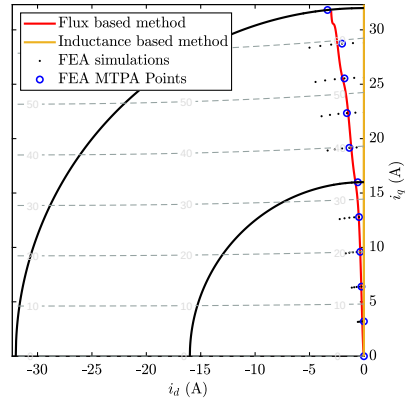

Fig. 8. MTPA control trajectories obtained for the SPM machine.

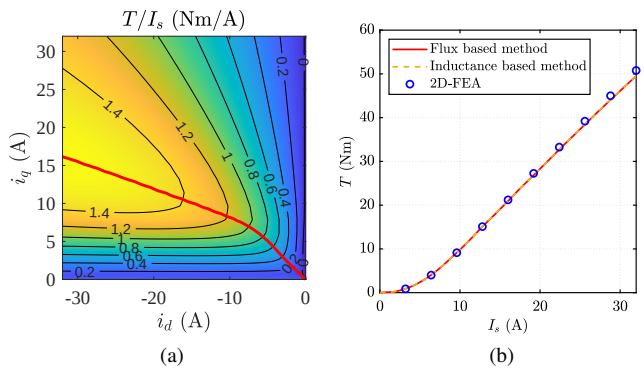

Fig. 7. a) Ratio of the torque and the current module of the SyR motor in the $i_d - i_q$ plane, b) Torque versus current module in MTPA conditions for the SyR machine.

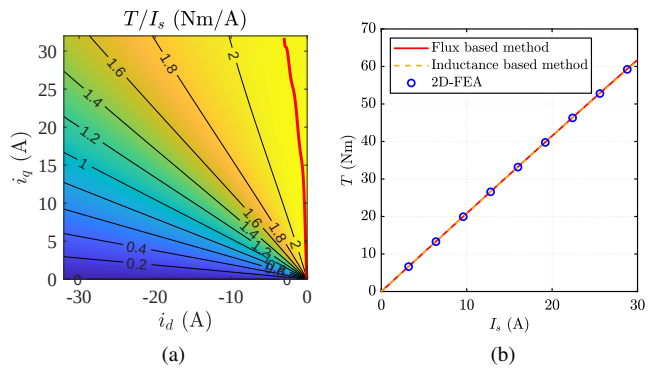

Fig. 9. a) Ratio of the torque and the current module of the SPM motor in the $i_d - i_q$ plane, b) Torque versus current module in MTPA conditions for the SPM machine.

the same for all the trajectories, since both the trajectories are inside the MTPA region.

VI. Conclusions

When a non-linear motor magnetic model is considered, the MTPA control trajectory cannot be computed analytically. In this paper, different approaches are compared to highlight the differences between each method applied to different machine topologies. The use of a non-linear magnetic model lead to a different interpretation of the MTPA trajectory since it appears more like a region instead of a line.

The first method computes the torque considering the inductances and keeping constant the flux generated by the magnets (see Eq. 2). The MTPA trajectory is found with a numeric algorithm which look for the maximum torque produced for a given current vector changing the current angle.

The second method presented is based directly on the torque map in the $i_d - i_q$ plane and compute the MTPA locus identifying the maximum torque along each current contour.

The obtained trajectories are validated via 2-D FEA simulations. The methods give both good results since the machine MTPA operating region is always encountered, but some difference are highlighted especially for the SPM machine and the PM-SyR machine at overload operating conditions. The flux based approach is more accurate according to 2-D FEA simulations results.

The two computation methods are validated against the MTPA computed from 2D-FEA simulations on four benchmark motor. The validation confirm the accuracy of the proposed methods, as the three MTPA trajectories are quite perfectly superimposed. This accuracy is confirmed by the four benchmark motors, that presents a different mix of magnetic anisotropy and PM strength.

Besides the MTPA locus accuracy, the validation shows that the sensitivity of torque on the current angle is low around the MTPA locus, reducing the effects of bad MTPA tracking. Indeed, the T/I ratio in the dq plane presents quite a flat behavior around the MTPA line for all the machines, except the low-PM-content machines at low current (when the magnetizing current component is relevant). This behavior makes the torque-current curves along the MTPA almost perfectly superimposed for all the presented methods, even if the dq trajectories are slightly different.

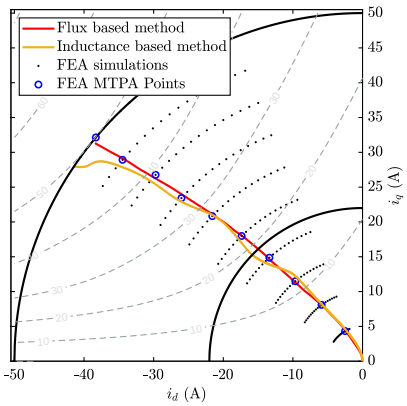

Fig. 10. MTPA control trajectories obtained for the PM-SyR machine.

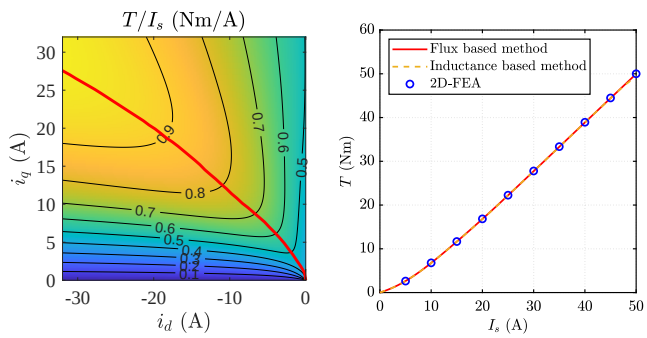

(a) (b)

Fig. 11. a) Ratio of the torque and the current module of the SPM motor in the $i_d - i_q$ plane, b) Torque versus current module in MTPA conditions for the PM-SyR machine.

References

[1] Z. Yang, F. Shang, I. P. Brown, and M. Krishnamurthy, "Comparative study of interior permanent magnet, induction, and switched reluctance motor drives for EV and HEV applications," *IEEE Transactions on Transportation Electrification*, vol. 1, no. 3, pp. 245–254, 2015.

[2] B. Sarlioglu and C. T. Morris, "More electric aircraft: Review, challenges, and opportunities for commercial transport aircraft," *IEEE Transactions on Transportation Electrification*, vol. 1, no. 1, pp. 54–64, 2015.

[3] G. Sulligoi, A. Vicenzutti, and R. Menis, "All-electric ship design: From electrical propulsion to integrated electrical and electronic power systems," *IEEE Transactions on Transportation Electrification*, vol. 2, no. 4, pp. 507–521, 2016.

[4] S. MacMinn and T. Jahns, "Control techniques for improved high-speed performance of interior PM synchronous motor drives," in *Conference Record of the 1988 IEEE Industry Applications Society Annual Meeting*, 1988, pp. 272–280 vol.1.

[5] A. Consoli, G. Scarcella, G. Scelba, and S. Sindoni, "Modeling control of IPM synchronous motors," in *2008 IEEE Power and Energy Society General Meeting - Conversion and Delivery of Electrical Energy in the 21st Century*, 2008, pp. 1–6.

[6] S. Calligaro, D. Marzona, R. Petrella, and A. Shahdadi, "MTPA tracking algorithms for ipmsms and synrms: Accurate evaluation and adaptive tuning of real signal injection and virtual signal injection," in *2020 IEEE Energy Conversion Congress and Exposition (ECCE)*, 2020, pp. 6079–6086.

[7] S. Morimoto, M. Sanada, and Y. Takeda, "Effects and compensation of magnetic saturation in flux-weakening controlled permanent magnet synchronous motor drives," *IEEE Transactions on Industry Applications*, vol. 30, no. 6, pp. 1632–, 1994.

[8] Z. Li, D. O'Donnell, W. Li, P. Song, A. Balamurali, and N. C. Kar, "A comprehensive review of state-of-the-art maximum torque per ampere strategies for permanent magnet synchronous motors," in *2020 10th International Electric Drives Production Conference (EDPC)*, 2020, pp. 1–8.

[9] H.-S. Kim, Y. Lee, S.-K. Sul, J. Yu, and J. Oh, "Online MTPA control of IPMSM based on robust numerical optimization technique," *IEEE Transactions on Industry Applications*, vol. 55, no. 4, pp. 3736–3746, 2019.

[10] A. Consoli, G. Scarcella, G. Scelba, and A. Testa, "Steady-state and transient operation of IPMSMs under maximum-torque-per-ampere control," *IEEE Transactions on Industry Applications*, vol. 46, no. 1, pp. 121–129, 2010.

[11] FEMM by David Meekers .

[12] S. Ferrari, G. Pellegrino, M. Davoli, and C. Bianchini, "Reduction of torque ripple in synchronous reluctance machines through flux barrier shift," in *2018 XIII International Conference on Electrical Machines (ICEM)*, 2018, pp. 2290–2296.

[13] S. Ferrari and G. Pellegrino, "FEAfix: FEA refinement of design equations for synchronous reluctance machines," *IEEE Transactions on Industry Applications*, vol. 56, no. 1, pp. 256–266, 2020.

[14] C. Lu, S. Ferrari, G. Pellegrino, C. Bianchini, and M. Davoli, "Parametric design method for SPM machines including rounded PM shape," in *2017 IEEE Energy Conversion Congress and Exposition (ECCE)*, 2017, pp. 4309–4315.

[15] S. Ferrari, E. Armando, and G. Pellegrino, "Torque ripple minimization of PM-assisted synchronous reluctance machines via asymmetric rotor poles," in *2019 IEEE Energy Conversion Congress and Exposition (ECCE)*, 2019, pp. 4895–4902.

[16] Simone Ferrari and Gianmario Pellegrino, "SyR-e/syre_public: SyR-e v3.8.2," Oct. 2024. [Online]. Available: https://zenodo.org/doi/10.5281/zenodo.13944455

[17] C. Bianchini, G. Bisceglie, A. Torreggiani, M. Davoli, E. Macrelli, A. Bellini, and M. Frigieri, "Effects of the magnetic model of interior permanent magnet machine on MTPA, flux weakening and MTPV evaluation," *Machines*, vol. 11, no. 1, 2023. [Online]. Available: https://www.mdpi.com/2075-1702/11/1/77